

AUTONOMOUS LUNAR ORBIT NAVIGATION USING OPTICAL SENSORS

Sun Hur-Diaz^{*}, Bill Bamford[†], Dave Gaylor[§]

Autonomous use of optical sensors for obtaining self-contained navigation solutions in a lunar orbit that are independent of ground or other external aids is explored. Tracking of multiple unknown landmarks on the Moon is considered along with a disk measurement providing range information from infrared sensors. Sensitivity of the navigation performance to sensor accuracy, measurement frequency, and initial error is assessed. Navigation performance obtained from tracking unknown landmarks is compared with performance obtained from tracking known landmarks.

INTRODUCTION

With the exploration of the Moon under NASA's Constellation Program, there is an increased interest in innovative navigation systems that are autonomous and reliable. This paper explores the navigation accuracy that can be obtained in lunar orbit using visible and infrared optical sensors in a self-contained manner that is independent of ground or other external aids. For greater autonomy and flexibility, tracking of unknown landmarks on the Moon is considered using the visible camera along with disk measurements from infrared detectors for range information. Tracking unknown landmarks, as opposed to known landmarks, requires additional states to solve for in the navigation algorithm, but does not necessitate storing a separate catalog of landmarks and employing a landmark identification algorithm.

In this paper, sensitivity of the navigation performance to sensor accuracy, measurement frequency, and initial error is assessed. An Extended Kalman Filter (EKF) with a high-fidelity implementation of the lunar orbit using the LP165P lunar gravity model is used to estimate the position and velocity of a spacecraft in a low-lunar orbit. Navigation performance obtained from tracking unknown landmarks is compared with performance obtained from tracking known landmarks.

^{*} Emergent Space Technologies, Inc., Greenbelt, MD 20770. E-mail: sun.hur-diaz@emergentspace.com.

[†] Emergent Space Technologies, Inc., Greenbelt, MD 20770. E-mail: bill.bamford@emergentspace.com.

[§] Emergent Space Technologies, Inc., Greenbelt, MD 20770. E-mail: dave.gaylor@emergentspace.com.

METHODOLOGY

The position and velocity of a spacecraft in a lunar orbit are estimated from optical measurements with an extended Kalman filter (EKF). The use of the EKF has been well documented in the literature (e.g., Gelb¹) and is only briefly described below followed by the description of the optical measurements used.

Extended Kalman Filter

Given the equations of motion and measurement data, an EKF can provide a minimum variance estimate of the spacecraft position, velocity and other state variables such as the lunar-fixed coordinates of an unknown landmark. The basic equations are summarized below.

The general non-linear state propagation model is represented by:

$$\dot{\bar{x}}(t) = \bar{f}(\bar{x}(t), t) + G(t)\bar{w}(t) \quad (1)$$

where the states \bar{x} are the inertial position and velocity of the spacecraft and the position of an unknown landmarks in selenographic coordinate frame (i.e., lunar-fixed):

$$\bar{x} \equiv \begin{bmatrix} \bar{r} \\ \bar{v} \\ \bar{x}_{LMF} \end{bmatrix} \equiv \begin{bmatrix} x \\ y \\ z \\ u \\ v \\ w \\ x_{LMF} \\ y_{LMF} \\ z_{LMF} \end{bmatrix} \quad (2)$$

The process noise \bar{w} is assumed to have normal distribution with zero mean and spectral density Q : $\bar{w}(t) \sim N(0, Q(t))$. The general non-linear measurement model is represented by:

$$\bar{z}_k = \bar{h}(\bar{x}_k) + \bar{v}_k \quad (3)$$

where the measurement noise is assumed to have zero mean and covariance R_k : $\bar{v}_k \sim N(0, R_k)$. The EKF formulation requires linearization of these models at each measurement time step. Accordingly, we define the output and system matrices as:

$$H_k \equiv \left. \frac{\partial \bar{h}}{\partial \bar{x}} \right|_{\bar{x}=\hat{x}} \quad F \equiv \left. \frac{\partial \bar{f}}{\partial \bar{x}} \right|_{\bar{x}=\hat{x}} \quad (4)$$

Between measurements, the state and covariance are propagated using the following equations:

$$\begin{aligned}\dot{\hat{x}}(t) &= \bar{f}(\bar{x}(t), t) \\ \dot{\Phi}(t_k, t_{k-1}) &= F(t_{k-1})\Phi(t_k, t_{k-1}) \\ P_k^- &= \Phi(t_k, t_{k-1})P_k^+\Phi^T(t_k, t_{k-1}) + Q_k\end{aligned}\quad (5)$$

where Φ is the state transition matrix. When measurements are available, the state and covariance are updated using the following equations:

$$\begin{aligned}\hat{x}_k^+ &= \hat{x}_k^- + K_k[\bar{z}_k - \bar{h}(\hat{x}_k^-)] \\ P_k^+ &= [I - K_k H_k(\hat{x}_k^-)]P_k^-\end{aligned}\quad (6)$$

where the Kalman gain is given by:

$$K_k = P_k^- H_k^T [H_k P_k^- H_k^T + R_k]^{-1}\quad (7)$$

Measurements

Two types of measurements from the optical sensor (camera) are considered for navigation in lunar orbit. First is the angle between a landmark on the Moon and an inertial reference. Second is the disk measurement of the Moon.

Angle Measurement. An inertial reference can be a star whose inertial position is known. If the field-of-view (FOV) of the camera is large enough, the star and the landmark can be viewed simultaneously, and the measurements are susceptible mainly to the camera-related errors. Since the position of the star that is sighted with the landmark has to be known, a star catalog and a star-identification algorithm are required. Alternatively, if the inertial attitude of the spacecraft, and hence the sensor, is known from a separate star tracker and gyros, then the camera coordinates themselves can be used as the inertial references. This method is susceptible to any star tracker and gyro errors as well as any misalignments relative to the optical sensor. Since the star tracker is an optical sensor itself, it can be used for landmark tracking as well, but the desired pointing for landmarks will be opposite that for star sensing for attitude determination. In this paper, the inertial attitude of the optical sensor is assumed known, and the inertial references will be the sensor axes.

The angle measurement equation is derived by first assuming a star inertial reference, then extending it to the sensor coordinate frame. For simplicity, the sensor coordinate frame is assumed co-aligned and centered with the spacecraft coordinate frame. The

angle measurement can be obtained from the inner product of the Line-of-Sight (LOS) vector measurements to the two objects in the sensor frame:

$$z_{\text{ANGLE}} = \cos \theta = [\hat{u}_1]_{\text{Sensor}}^T [\hat{u}_2]_{\text{Sensor}} \quad (8)$$

where θ is the angle between the two LOS vectors. The basic geometry for this measurement type is shown in Figure 1.

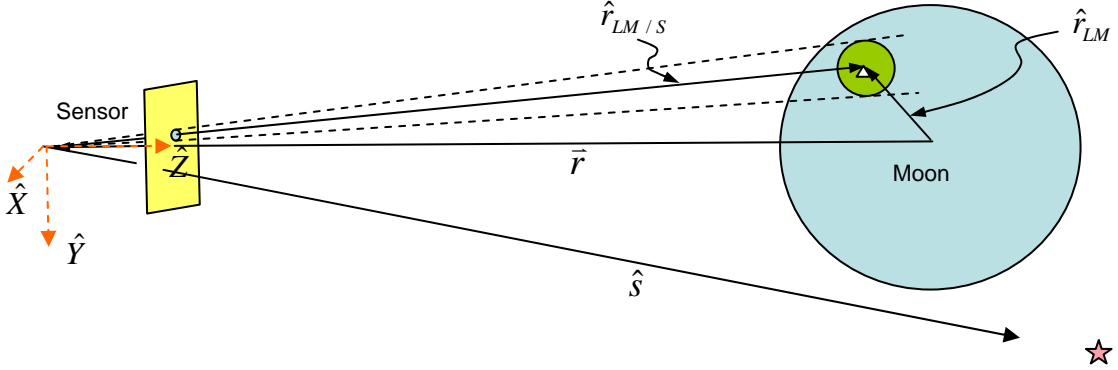


Figure 1 Angular optical measurement

The vector \vec{r} is from the Moon to the spacecraft and is part of the EKF state to be estimated. The vector $\hat{r}_{LM/S}$ is from the spacecraft to the landmark and is one of the unit vectors measured by the sensor. The remaining vectors shown in the figure are \vec{r}_{LM} from the Moon to the landmark and \hat{s} , the unit vector from the spacecraft to the star as measured by the sensor. So in Eq. (8), the first unit vector is derived from the (X_{LM}, Y_{LM}) angular coordinates of the landmark in the focal plane:

$$\hat{u}_1 = \frac{\begin{bmatrix} \tan(X_{LM}) \\ \tan(Y_{LM}) \\ 1 \end{bmatrix}}{\sqrt{\tan^2(X_{LM}) + \tan^2(Y_{LM}) + 1}} \quad (9)$$

Similarly, the second unit vector in Eq. (8) can be derived from the focal plane angular coordinates of the star. Unit vector computation can be bypassed by computing the angle between the landmark image and the star image directly from spherical trigonometry and taking the cosine of the angle.

If the inertial attitude of the camera is known, then the \hat{X} and the \hat{Y} unit vectors of the camera coordinate frame itself can both be used as the second unit vector in Eq. (8). The same inner product equation applies, so that

$$\begin{aligned} z_{ANGLE1} &= \hat{u}_1(1) \\ z_{ANGLE2} &= \hat{u}_1(2) \end{aligned} \quad (10)$$

where the elements of the unit vector \hat{u}_1 is given by Eq. (9).

To formulate the measurement equation in terms of the states, the \hat{u}_1 is computed in terms of the inertial position vector from the Moon to the sensor, \vec{r} , and the position of the landmark relative to the Moon, \vec{x}_{LMF} :

$$[\hat{u}_1]_{Inertial} = \hat{r}_{LM/S} = \frac{T_{I/F} \vec{x}_{LMF} - \vec{r}}{|T_{I/F} \vec{x}_{LMF} - \vec{r}|} \quad (11)$$

where $T_{I/F}$ is the transformation from the lunar-fixed coordinate frame to the inertial frame. Since the transformation matrix from the inertial frame to the sensor frame is known,

$$T_{S/I} = \begin{bmatrix} \hat{X}_I^T \\ \hat{Y}_I^T \\ \hat{Z}_I^T \end{bmatrix} \quad (12)$$

derived from the known inertial attitude, the equation for the landmark angular measurement is given by

$$\begin{aligned} h_{ANGLE1} &= \hat{X}_I^T \hat{r}_{LM/S} \\ h_{ANGLE2} &= \hat{Y}_I^T \hat{r}_{LM/S} \end{aligned} \quad (13)$$

Disk Measurement. Another type of measurement is the angle subtended by the disk of the Moon. Since the physical size of the Moon is known, the distance between the camera and the Moon can be deduced from this measurement. The geometry for this measurement type is shown below.

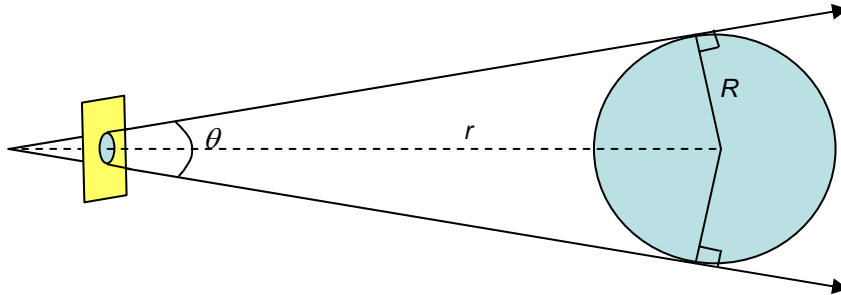


Figure 2 Geometry for disk measurement

The measurement is the sine of half of the subtended angle

$$z_{DISK} = \sin\left(\frac{\theta}{2}\right) \quad (14)$$

which can be derived from the angular measurement of a circular template fitted to the image on the focal plane. The disk measurement can be written in terms of the distance to the Moon, r , as follows:

$$h_{DISK} = \frac{R}{r} = \frac{R}{\sqrt{x^2 + y^2 + z^2}} \quad (15)$$

Because of frequent night passes, this measurement type is most useful with an infrared sensor. The use of infrared sensors on the Moon has been considered for a very long time, see for example Falbel², where it is shown that the total radiance from the dark side of the Moon is about 4 times greater than the minimum detectable radiance of 0.1 milliwatts/cm²-ster. The total radiance from the light side of the Moon is 100 times greater than the dark side. The challenge is to have a detector that has the large range of sensitivity to cover both the dark and the light sides of the Moon to enable disk-range measurements at all times as the spacecraft orbits the Moon. Instead of an IR sensor, a radar altimeter can provide the same type of measurement; however, in this paper we are limiting ourselves to optical sensors. Landmark size measurements are possible as well, but this requires identification of the landmark and knowledge of its physical dimensions.

Landmark tracking

To simplify the Kalman filter with unknown landmarks, the position of only one landmark is estimated at a time. Therefore, when a given landmark goes out of the FOV, a new one is picked up and tracked. Whether a landmark is visible is determined from the following geometry.

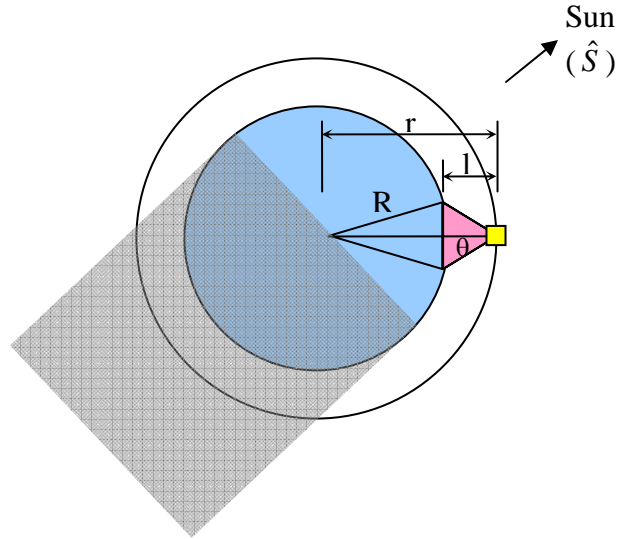


Figure 3 Geometry for computing landmark visibility

Since the spacecraft is assumed controlled to nadir-pointing, we assume that a landmark is in the FOV of the camera if the following condition is satisfied:

$$\hat{r}^T \hat{r}_{LM} > \frac{r-l}{R} \quad (16)$$

where

r = distance from the Moon to the spacecraft

R = radius of the Moon

l = distance from spacecraft to the plane intersecting
the camera cone with the Moon surface

$$= \frac{r - \sqrt{r^2 - (1 + \tan^2 \theta)(r^2 - R^2)}}{1 + \tan^2 \theta}$$

θ = camera FOV half angle

For a landmark to be tracked by the visible optical sensor, it also needs to be illuminated. A landmark is illuminated if the following condition is satisfied:

$$\hat{S}^T \hat{r}_{LM} > 0 \quad (17)$$

Once a landmark is acquired by the sensor, the initial guess of its lunar-fixed coordinates to input into the Kalman filter is derived from the current estimate of the spacecraft position, the inertial attitude of the sensor, and the angular position of the landmark itself in the focal plane. First the unit vector to the landmark from the sensor in the sensor frame, $[\hat{r}_{LM/S}]_{sensor}$, is given by Eq. (9). In Figure 3, if the sensor FOV half-angle θ is replaced by the measured landmark's cone angle from the sensor boresight,

$$\theta_{LM} = \arccos(\cos X_{LM} \cos Y_{LM}) \quad (18)$$

then the vector from the sensor to the landmark can be estimated to be

$$[\bar{r}_{LM/S}]_{Sensor} = \frac{l_{est}}{\cos \theta_{LM}} [\hat{r}_{LM/S}]_{Sensor} \quad (19)$$

where l_{est} is computed from the current estimate of the spacecraft position, \bar{r}_{est} . With the inertial attitude of the sensor known, this unit vector can be rotated into the inertial frame and combined with the current estimate of the sensor (spacecraft) position relative to the Moon to obtain the landmark's lunar-fixed coordinates:

$$[\bar{x}_{LMF}]_{est} = T_{F/I} \left(\bar{r}_{est} + T_{I/S} [\bar{r}_{LM/S}]_{Sensor} \right) \quad (20)$$

where $T_{I/S}$ is the transformation from the sensor frame to the inertial frame which is the transpose of what was given in Eq. (12), and $T_{F/I}$ is the transformation matrix from the inertial frame to the lunar-fixed frame whose formulation can be obtained from references such as Escobal³. This then becomes the initial landmark position estimate corresponding to the newly acquired landmark.

RESULTS

As an example, we consider a spacecraft in a low-lunar circular polar orbit with an altitude of 100 km whose orbit period is about 2 hours. At this altitude, the maximum visibility duration of any single landmark is approximately 12 minutes. The true orbit is propagated with the effects of the Moon's gravity using the LP165P gravity model. This model was derived from radio tracking of the Lunar Orbiter 1 to 5, Apollo 15 and 16 subsatellites, Clementine, and all the data (Jan 11, 1998 to July 30, 1999) of the Lunar Prospector spacecraft (Ref. 4).

The mean rotational period of the moon is 27.3 days. So in 2 days, the moon rotates about 26 degrees. Figure 4 shows the orbit in selenographic and inertial coordinate frames over 2 days. The spacecraft will spend about half its time in the Moon's shadow where visible optical imaging of the lunar surface is not possible.

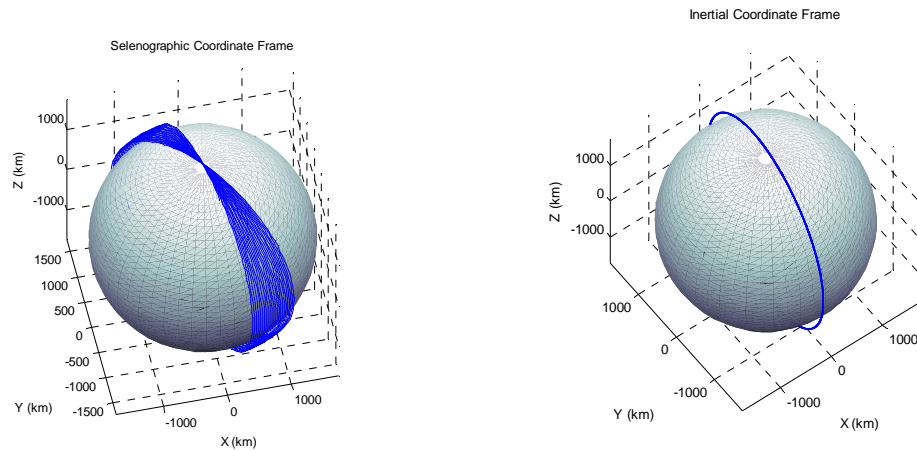


Figure 4 Low Lunar orbit in selenographic and inertial coordinate frames

Two possible scenarios for landmark tracking are considered. One is where we assume the sensor is strictly nadir pointing and a landmark is tracked as long as it is in the FOV of the sensor. The other is where we assume the sensor can slew to follow the landmark until it disappears from the horizon. The two scenarios will be referred to as FOV-tracking and horizon-tracking, respectively. In both, it is assumed that a new landmark is acquired as soon as the current one is no longer visible. For simplicity, instantaneous slewing to the starting horizon is assumed for the horizon-tracking scenario. In reality, it would take a finite time to slew the sensor back to start tracking a new landmark. Theoretically, if the FOV of the sensor is large enough to span the horizon, then slewing is not required. In the simulations, horizon tracking is implemented in this manner.

The initial orbit for the simulations was selected such that during roughly half the orbit, the sensor is on the dark side of the Moon so that no visible landmark tracking can be made. If the orbit was along the terminator of the Moon, on the other hand, continuous landmark tracking is a possibility. Illumination of the Moon as seen by the sensor is shown in Figure 5.

In addition to landmark tracking, we can introduce infrared disk measurements. For the 100 km altitude orbit considered in this study, the Moon subtends an angle of 142 deg. This large angle sensing can be accommodated with mirrors or with arrays of IR detectors. One such arrayed IR sensor is described in Reference 5. False limb detections due to terminator crossing or shadows on the lunar surface can be avoided by scanning from the outer-most detector which senses the cold space towards the inner-most detector.

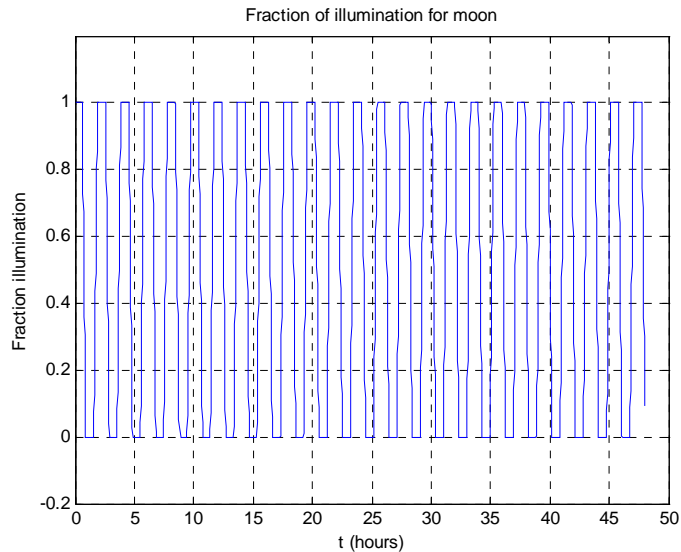


Figure 5 Fraction of illumination of the Moon as seen by the sensor in its orbit

Simulation Parameters

Parameters that were varied in this navigation study and their values are:

1. Tracking method
 - a. FOV-Tracking (70 deg example)
 - b. Horizon-Tracking
2. Landmark knowledge
 - a. Known
 - b. Unknown (solve for landmark position in EKF)
3. Landmark measurement accuracy (1σ)
 - a. Do not use
 - b. 0.1 deg
 - c. 0.01 deg
4. Disk measurement accuracy
 - a. Do not use
 - b. 1 deg
 - c. 0.1 deg (typical of Earth sensor)
5. Measurement sample period
 - a. 60 sec
 - b. 1 sec
6. Initial position and velocity errors along Radial-Tangential-Normal (RTN) directions
 - a. 10 km, 10 m/s each direction
 - b. 100 km, 100 m/s each direction

We focus on the sensitivity of each parameter relative to a nominal case. The nominal case is defined here to be:

- Horizon-tracking
- Unknown landmarks
- Landmark measurement accuracy of 0.1 deg
- Disk measurement accuracy of 0.1 deg
- Both sampled every 60 seconds
- Initial estimate error of 10 km and 10 m/s in each RTN direction.

A 10x10 lunar gravity model was used for the truth, and a 4x4 model was used for the Kalman filter.

The position and velocity estimation errors, as well as the landmark estimation error, for the nominal case are shown in Figure 6. The RMS and maximum position errors during the second day are 1.4 and 2.8 km, respectively. The RMS and maximum velocity errors during the same period are 1.2 and 2.6 m/s, respectively.

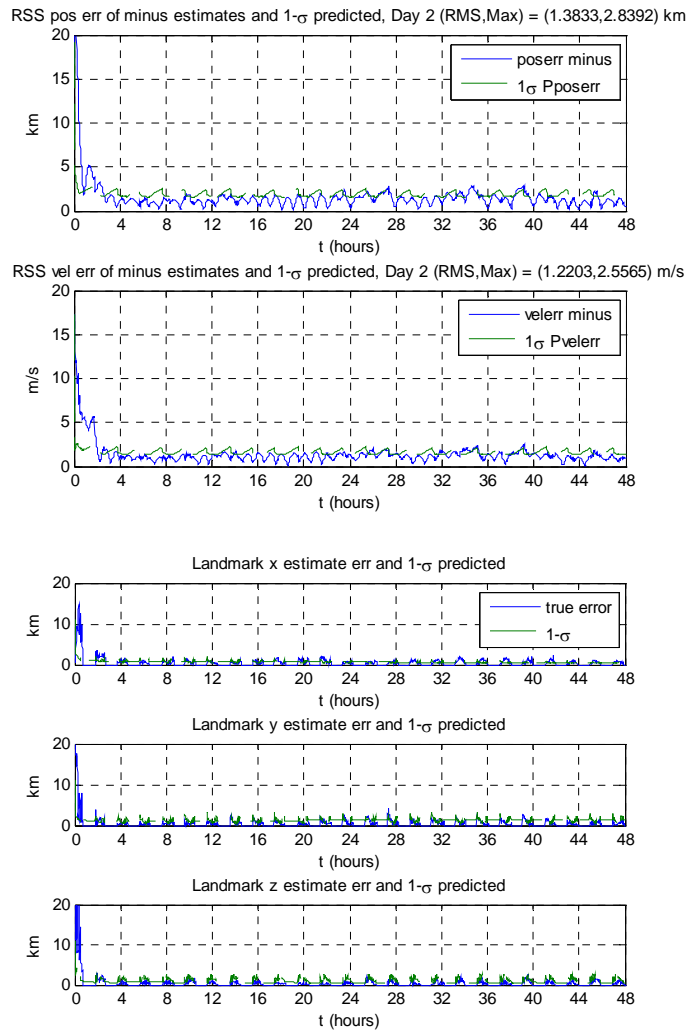


Figure 6 Nominal case performance

Each of the six parameters described earlier were then varied and the resulting performance was compared with the nominal case. In all of the subsequent plots, the two numbers shown in parenthesis in the legend indicate RMS and maximum errors during the second half of the simulation.

FOV-Tracking

We assume a 70 deg FOV with the sensor strictly nadir-pointing. Accordingly, a given landmark is tracked for only about two measurements at the 60 second sample time versus about ten measurements for the horizon-tracking method. The position and velocity estimate errors for both the FOV-tracking and the nominal horizon-tracking are shown in Figure 7. The RMS and maximum errors are slightly higher at 2.0 and 3.3 km for position and 1.7 and 3.2 m/s for velocity.

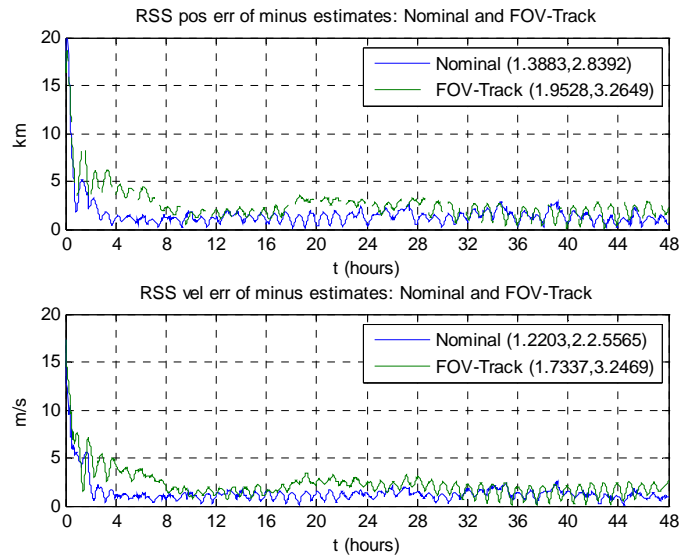


Figure 7 Comparison of FOV-tracking versus horizon-tracking (nominal case)

Known Landmarks

The same horizon-tracking method is used in this case except the landmark positions are assumed to be known. Therefore, the total number of Kalman filter states is reduced to six. The results are shown in Figure 8. The known landmark case performance is better by almost a factor of two.

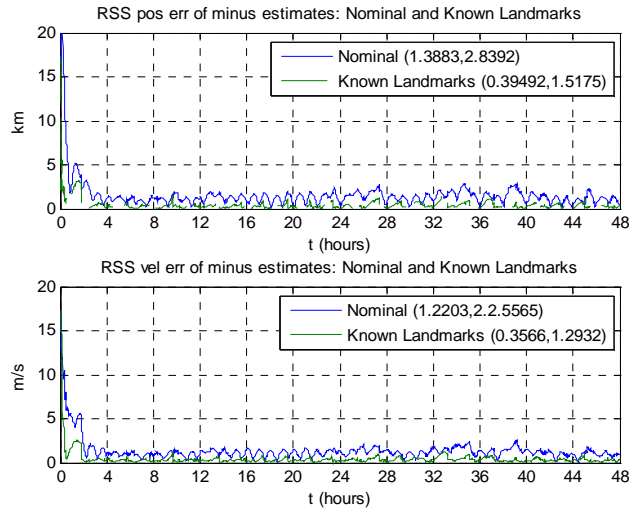


Figure 8 Comparison of known versus unknown landmarks (nominal case)

Landmark Measurement Accuracy

In the nominal case, the landmark measurement accuracy of 0.1 deg was used. This corresponds roughly to a medium accuracy sensor of about 100 deg FOV with a 1024 by 1024 pixel array. A high accuracy sensor with a 10 deg FOV with the same number of pixels would provide measurements that are 10 times more accurate. The Kalman filter performance for this level of accuracy in the landmark measurement is shown in Figure 9. Also shown in the figure is the nominal case, as well as a case with no landmark measurements, i.e., using only the nominal accuracy (0.1 deg) disk measurements. Reducing the landmark measurement accuracy by a factor of 10 improves the performance by roughly a factor of two. Using disk measurements alone gives poor performance.

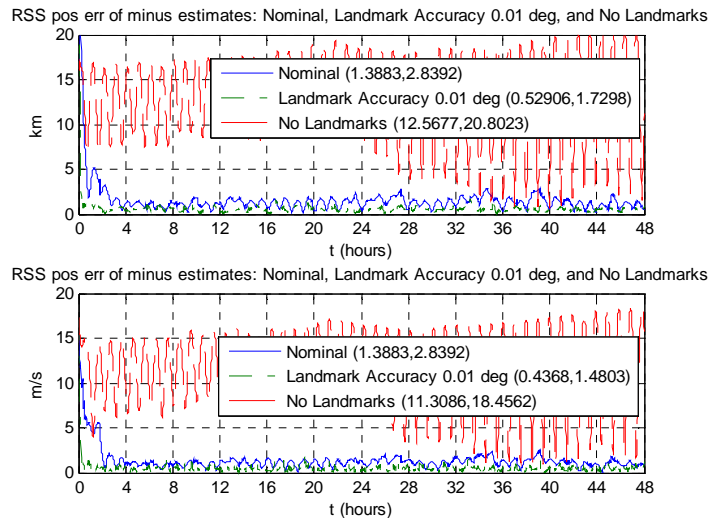


Figure 9 Comparison of landmark measurement accuracy of 0.01 deg and no landmarks (disk only) against the landmark accuracy of 0.1 deg (nominal case)

Disk Measurement Accuracy

In the nominal case, disk measurements with an accuracy of 0.1 deg was used. The navigation performance with the disk accuracy 10 times worse is shown in Figure 10 with the nominal case. Also shown is the performance with no disk measurements which is only slightly worse than the nominal in the steady-state performance, although the convergence takes longer. Using inaccurate disk measurements, on the other hand, results in much worse performance.

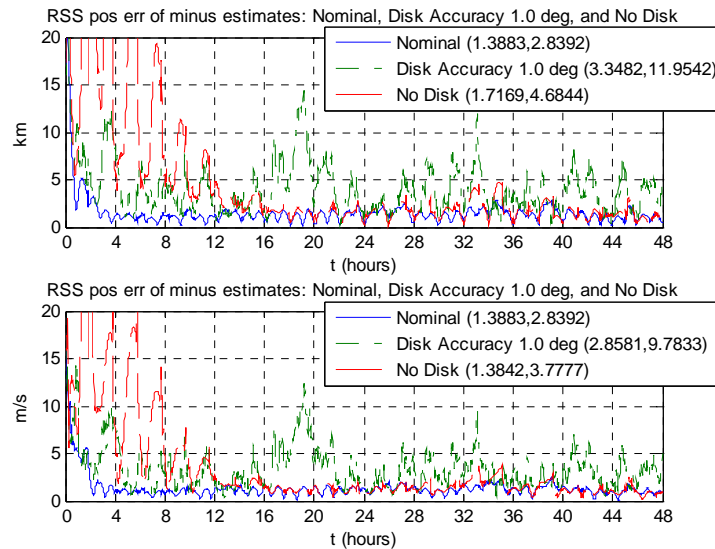


Figure 10 Comparison of disk measurement accuracy of 1.0 deg and no disk (landmarks only) against disk measurement accuracy of 0.1 deg (nominal case)

Measurement Sample Period

Shortening the time between measurements in a Kalman filter improves performance. This is evident in Figure 11 where a 1-sec sampling case is compared with the nominal 60-sec sampling case. The 1-sec case is better by roughly five times in the RMS. Although the navigation performance is improved, increasing sampling frequency increases the load on the onboard flight processor.

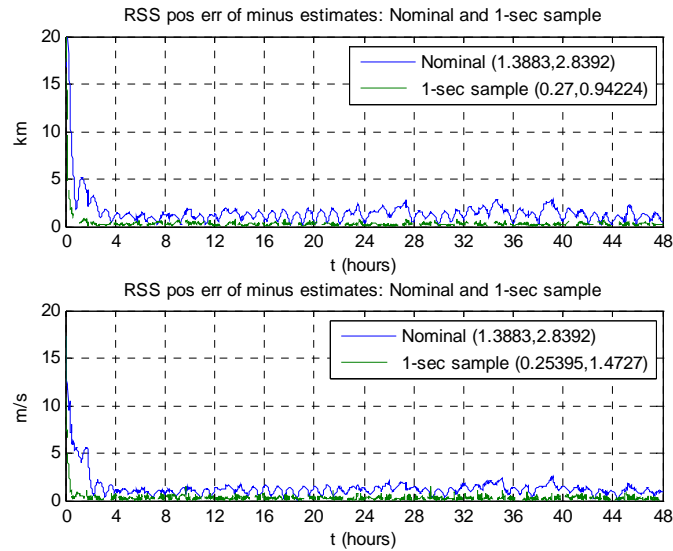


Figure 11 Comparison of 1-sec sampling versus 60-sec sampling (nominal case)

Initial Estimate Error

The final parameter that is considered for variation is the initial estimate error. The nominal case had an initial error 10 km and 10 m/s in each direction of the RTN coordinate frame. Figure 12 shows the performance with a factor of 10 increase in the initial position and velocity errors. Although the convergence takes longer, the steady-state performance difference is negligible.

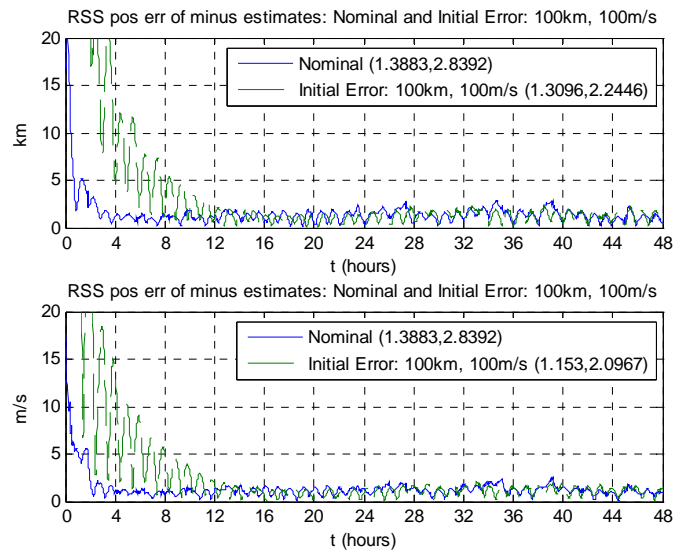


Figure 12 Comparison of 100km and 100m/s initial estimate error versus the 10km and 10m/s (nominal case)

CONCLUSIONS

Autonomous navigation in lunar orbit using optical sensors was investigated in this paper. The methodology involves tracking of a single landmark at a time, but continuously acquiring a new one when the old one drops from visibility of the optical sensor. Two measurement types were considered: visible angular measurement of the landmark relative to an inertial reference and infrared disk measurement of the Moon. Six parameters of interest were varied individually to determine their sensitivity relative to a nominal case. These parameters were tracking method (FOV vs. horizon), landmark position knowledge (known vs. unknown), landmark measurement accuracy, disk measurement accuracy, measurement sample period, and initial estimate error.

Table 1 summarizes the steady-state RMS errors of these parameter variations. The worst performing of all the variations was the one where no landmark measurements were used followed by the case where the disk measurement accuracy was increased to 1.0 deg. There were very little differences from the nominal for two cases: no disk measurements and initial errors of 100 km and 100 m/s, while switching from horizon-tracking to FOV-tracking gave a slightly worse performance. Decreasing the unknown landmark measurement accuracy to 0.01 deg or decreasing the measurement sample period to 1 second gave similar performance as using known landmarks with measurement accuracy of 0.1 deg. These three parameter variations had steady-state RMS errors roughly three times smaller than the nominal case.

To really characterize the navigation performance with the different combinations of parameters, a Monte Carlo study needs to be done. However, the parametric simulation study described in this paper shows the relative benefits of each parameter variation and that less than 2 km RMS position error can be obtained in most cases.

Table 1 STEADY STATE NAVIGATION ACCURACY

Case	Position RMS (km)	Velocity RMS (m/s)
<u>Nominal</u> Horizon-Tracking Unknown Landmarks Landmark Measurement Accuracy 0.1 deg Disk Measurement Accuracy 0.1 deg Sample Period 60 sec Initial Estimate Error 10 km, 10 m/s	1.4	1.2
FOV-Tracking	2.0	1.7
Known Landmarks	0.4	0.4
No Landmarks	12.6	11.3
Landmark Measurement Accuracy 0.01 deg	0.5	0.4
No Disk	1.7	1.4
Disk Measurement Accuracy 1.0 deg	3.3	2.9
Sample Period 1 sec	0.3	0.3
Initial Estimate Error 100 km, 100 m/s	1.3	1.2

REFERENCES

1. Gelb, A., *Applied Optimal Estimation*, The MIT Press, Cambridge, MA, 1974.
2. Falbel, Gerald and Robert Astheimer, "Infrared Horizon Sensor Techniques for Lunar and Planetary Approaches," AIAA Guidance and Control Conference, Massachusetts Institute of Technology, Cambridge, MA, August 12-14, 1963.
3. Escobal, P. R., *Methods of Orbital Determination*, John Wiley and Sons, NY, 1965.
4. Konopliv, A. S., S. W. Asmar, E. Carranza, W. L. Sjogren, and D. N. Yuan, "Recent Gravity Models as a Result of the Lunar Prospector Mission," *Icarus*, 150, 2001, p. 1-18.
5. van Herwaarden, A.W., "Low-Cost Satellite Attitude Control Sensors Based on Integrated Infrared Detector Arrays," *IEEE Transactions on Instrumentation and Measurement*, Vol. 50, No. 6, December 2001, p. 1524-1529.